Inkjet printed doped polyaniline: navigating through physics and chemistry for the next generation devices

Sergio Bocchini,[a] Micaela Castellino,[a] Cristina Della Pina,[b] Krishna Rajan,[a,c] Ermelinda Falletta,[b*] Alessandro Chiolerio,[a*]

[a] Center for Sustainable Future Technologies, Istituto Italiano di Tecnologia, corso Trento 21, 10129 Torino, Italy

[b] Dipartimento di Chimica, Università degli Studi di Milano, ISTM-CNR, via C. Golgi 19, 20133 Milano, Italy

[c] Applied Science and Technology Department, Politecnico di Torino, corso Duca degli Abruzzi 24, 10129 Torino, Italy

*Corresponding author: these authors contributed equally to this work

Abstract

Innovative benzidine-free PANI-based inks for electrically conductive inkjet printed devices were developed and tested and the results compared with those obtained by traditional PANI. NMR investigations evidenced the presence of quinones and phenolic groups on the backbone of the innovative PANIs that are thought being responsible for the higher solubility in DMSO. A mechanism of reaction was proposed. The numerous characterizations (NMR, UV-Vis, FTIR, XPS and electrical investigations) allowed to compare protonation level, doping level, valence band maximum for both the type of PANI.

The correlation among structural properties, printability, conductivity and solubility was discussed.

Keywords: polyaniline, films, inkjet printing

1. Introduction

Thanks to their unique properties, as electronic conductivity and easy preparation, intrinsically conducting polymers (ICPs) have become popular in many sectors ranging from tissue engineering[1] to regenerative medicine[2] and sensors[3].

Among the ICPs, polyaniline (PANI) occupies a special place owing to its environmental stability, interesting redox properties, simple synthesis, etc. that make it potentially useful for many applications. The most popular synthetic procedure for PANI preparation consists in the aniline monomer oxidative polymerization by stoichiometric oxidants. If on the one hand this approach leads to highly conducting polymer with good yield, on the other hand the production of toxic/carcinogenic coproducts (e. g., benzidine, *trans*-azobenzene, metals in high oxidation states, etc.) and inorganic waste in large amount limit its real application.

On the base of the pioneering investigations of Geniès and Kitani,[4, 5] a benzidine-free PANI was produced using *N*-(4-aminophenyl)aniline (aniline dimer) as the reagent maintaining the use of hard oxidants as the oxidizing agents.[6, 7] In order to totally avoid the production of toxic/mutagen substances and inorganic waste, we have recently investigated the possibility to produce PANI by the oxidative polymerization of *N*-(4-aminophenyl)aniline using hydrogen peroxide or molecular oxygen as the oxidizing agents in the presence of proper catalysts.[8-13] This innovative approach leads to H_2O as the unique inorganic co-product and eliminates the production of toxic species simplifying the polymer's post treatment.

Among numerous PANI-based materials applications, the possibility to develop thin films with desired properties and functionalities represents an important goal in many sectors. PANI films have been prepared by various methods, such as chemical oxidation, electrochemical synthesis, spin-coating and so on.[14-16] In this regard, printable PANI-based inks are particularly interesting for their application in conductive printed devices. Recently, some of the authors of the present work have focused their attention in the synthesis and characterization of printable polyanilines with good results.[6,7] Herein, we report our recent goals in the preparation of printable PANI-based inks using camphorsulfonic acid (CSA)- or aminosulfonic acid (AMSA)-doped PANI synthesized by a green protocol. The obtained innovative products were compared through many functional characterization techniques with samples obtained by CSA- and AMSA-doped PANI synthesized by a traditional protocol.

2. Experimental

2.1 Materials

All chemicals were used as received (Sigma Aldrich) without further purification unless stated otherwise.

2.2 PANIs preparation

Two different types of polyaniline and were prepared using a traditional (PANI1) and an innovative green approach (PANI2). Both the samples were dedoped (deprotonated) and redoped (reprotonated) by camphorsulfonic (CSA) and aminosulfonic (AMSA) acids obtaining four samples: PANI1/CSA (traditionally synthetized PANI doped with CSA), PANI2/CSA (green protocol synthetized PANI doped with CSA), PANI1/AMSA (traditionally synthetized PANI doped with AMSA) and PANI2/AMSA (green protocol synthetized PANI doped with AMSA).

2.2.1 Synthesis of PANI1-based materials

PANI1 was prepared on the base of a method reported in literature.[11] More in detail, 2.5 g (26.9 mmol) of aniline and 11 g (40.7 mmol) of $K_2S_2O_8$ were solubilized in 20 mL of HCl 2.5 M and in 40 mL of deionized water (DIW) respectively and cooled at 4°C.

The polymerization reaction took place with the dropwise addition of the oxidant aqueous solution. A green solid was collected by filtration after 6 hours. It was abundantly washed by water and acetone and dried under air. The product, obtained with a 73% yield, was spectroscopically characterized and identified as emeraldine salt (ES1). 1g of ES1 was undoped (deprotonated) by stirring in 10 mL of NH_4OH 1 M (10.0 mmol) for 24 hours. The resulting product, emeraldine base (EB1), was filtered, abundantly washed with water until the mother liquid became neutral and dried under air

Two portions of EB1 were separately dispersed in 80 mL of chloroform and stirred with 1.25 g of CSA and 0.52 g of AMSA (aniline/dopant = 2 molar ratio) respectively for 20 hours at room temperature. Then, the resulting soluble fractions of PANI1/CSA and PANI1/AMSA were recovered by filtration and dried under reduced pressure. The powdered samples were washed with acetonitrile in order to remove free dopant.

2.2.2 Synthesis of PANI2-based materials

In order to prepare PANI2 our previous synthetic protocol was followed.[17-19] 2 g (10.9 mmol) of *N*-(4-aminophenyl)aniline were solubilized in 50 mL of HCl 0.1 M at room temperature. Then, 1.87 g of H_2O_2 30% (5.67 mL) was quickly added immediately followed by 109 μL of a Fe^{+3} 0.01 M solution ($1.09 \cdot 10^{-2}$ mmol) acting as the reaction catalyst. The mixture was stirred for 24 hours. An insoluble green product was collected by filtration, abundantly washed by water and acetone and dried under

air. The product, obtained with an 82% yield, was spectroscopically characterized and identified as emeraldine salt (ES2). 1g of ES2 were undoped (deprotonated) by stirring in 10 mL of NH_4OH 1 M (10.0 mmol) for 24 hours. The resulting product, emeraldine base (EB2), was filtered, abundantly washed with water until the mother liquid became neutral and dried under air

Two portions of EB2 were separately dispersed in 80 mL of chloroform and stirred with 1.25 g of CSA and 0.52 g of AMSA (aniline/dopant = 2 molar ratio) respectively for 20 hours at room temperature. Then, the resulting soluble fractions of PANI2/CSA and PAN2/AMSA were recovered by filtration and dried under reduced pressure. The powdered samples were washed with acetonitrile in order to remove free dopant.

2.3 PANI inkjet printing process

The samples of doped PANI1 and PANI2 were prepared by dissolution in dimethyl sulfoxide (DMSO); all the solutions were saturated. The different solutions were filtered using a 450 nm size pores filter, then inserted into a 3 ml reservoir and loaded in the inkjet printing system (JETLAB 4-XL from Microfab, US). The system is equipped with independent heaters for the printing nozzle and the substrate, with the possibility of printing a maximum size of 21 x 26 cm^2. Printing tests were achieved through piezoelectric nozzles made in quartz, with a diameter of 80 µm, with a vibration frequency set to 250 Hz. The three-axis movement and the signal amplitude and waveform that command the piezoelectric nozzle were computer controlled, and the dimension and speed of ink drops were controlled by a horizontal camera located onto the x-y stage for direct drop observation. Jetting parameters were set as follows, using an asymmetrical pulse: first rise time 12 µs, dwell time 15 µs, fall time 5 µs, echo time 20 µs, second rise time 2 µs, idle voltage 0 V, dwell voltage 35 V, echo voltage -13 V. The nozzle and substrate holder were heated to a temperature of 40°C in order to obtain the correct value of ink viscosity, suitable for printing. Using the described printing setup, ink drops with diameter of ~100 µm were normally obtained. Consequently, the script used for test tracks printing was set to achieve a drop spacing of 100 µm to obtain complete coverage of the substrate. The total number of passes was kept at 6 or 10. For the electrical characterization, standard arrays of tracks having widths of 200 µm were used, depositing patterns at multiple passes. To measure conductivity we adopted a planar design in order to decouple the problem of fabricating controlled electrode gaps and have PANI deposition through the gap. This design has a planar structure with identical gold electrodes being deposited onto a silicon substrate, by means of an electron beam evaporator.

2.4 Characterization

The solubility of materials in dimethyl sulfoxide (DMSO) was evaluated dissolving 100 mg of each polymer in 50 ml of DMSO at 70 °C for 6 hours. Then, the insoluble part of each material was recovered by centrifugation, washed several times with DIW and dried in an oven at 110°C overnight. The loss of weight is the mass of the compound dissolved in the given volume of DMSO.

FT-IR spectra of KBr dispersed samples were collected by a JASCO FT/IR-410 spectrophotometer in the range of 500–4000 cm^{-1}. UV–vis spectra were collected on a Hewlett Packard 8453 spectrophotometer using DMSO as the solvent.

SEM images were recorded by a SEM LEO 1430 microscope.

^{1}H NMR spectra were recorded on a Bruker 400 MHz instrument using DMSO as the solvent.

XPS spectra were performed using A PHI 5000 Versaprobe scanning X-ray photoelectron spectrometer (monochromatic Al Kα X-ray source with 1486.6 eV energy). A spot size of 100 μm was used in order to collect the photoelectron signal for both the high resolution (HR) and the survey spectra. All samples were analyzed with a combined electron and Ar ion gun neutralizer system, in order to reduce the charging effect during the measurements. The semi-quantitative atomic compositions and deconvolution procedures were obtained using Multipak 9.6 dedicated software. All core-level peak energies were referenced to C1s peak at 284.5 eV and the background contribution in HR scans was subtracted by means of a Shirley function.

3. Results ad discussion

Before characterizing and processing all the samples, their solubility in DMSO was assessed at room temperature and the results are reported in the Table 1.

Synthesis route \ Composition (*n*)	**EB*n***	**PANI*n*/CSA**	**PANI*n*/AMSA**
1	**1.1**	**1.9**	**0.1**
2	**4.0**	**10.5**	**4.0**

Table 1: Solubility (expressed as mg/ml) of EB1, EB2, PANI1/CSA, PANI2/CSA, PANI1/AMSA and PANI2/AMSA in DMSO at room temperature.

PANI2-based samples are always more soluble than PANI1-based ones (from a minimum of 4 to a maximum of 40 times). Even though same authors relate this different behavior to difference in

molecular weights (lower for PANI2 than for PANI1),[4] other factors could be involved, such as little differences in chemical structure. Moreover, all PANIs protonated by CSA resulted to be more soluble than the corresponding AMSA-doped ones (from a minimum of 2.5 to a maximum of 20 times). This could be related on one hand to the small dimensions of AMSA if compared to CSA that reduce its ability to dissolve the materials and on the other hand to a low protonation level of PANIs when AMSA is used as the dopant, as confirmed by the FT-IR investigations (see § 3.2) and conductivity measurements (see § 3.4).

Chemical structure of both EB1 and EB2 was investigated by NMR analyses (Fig. 1).

a)

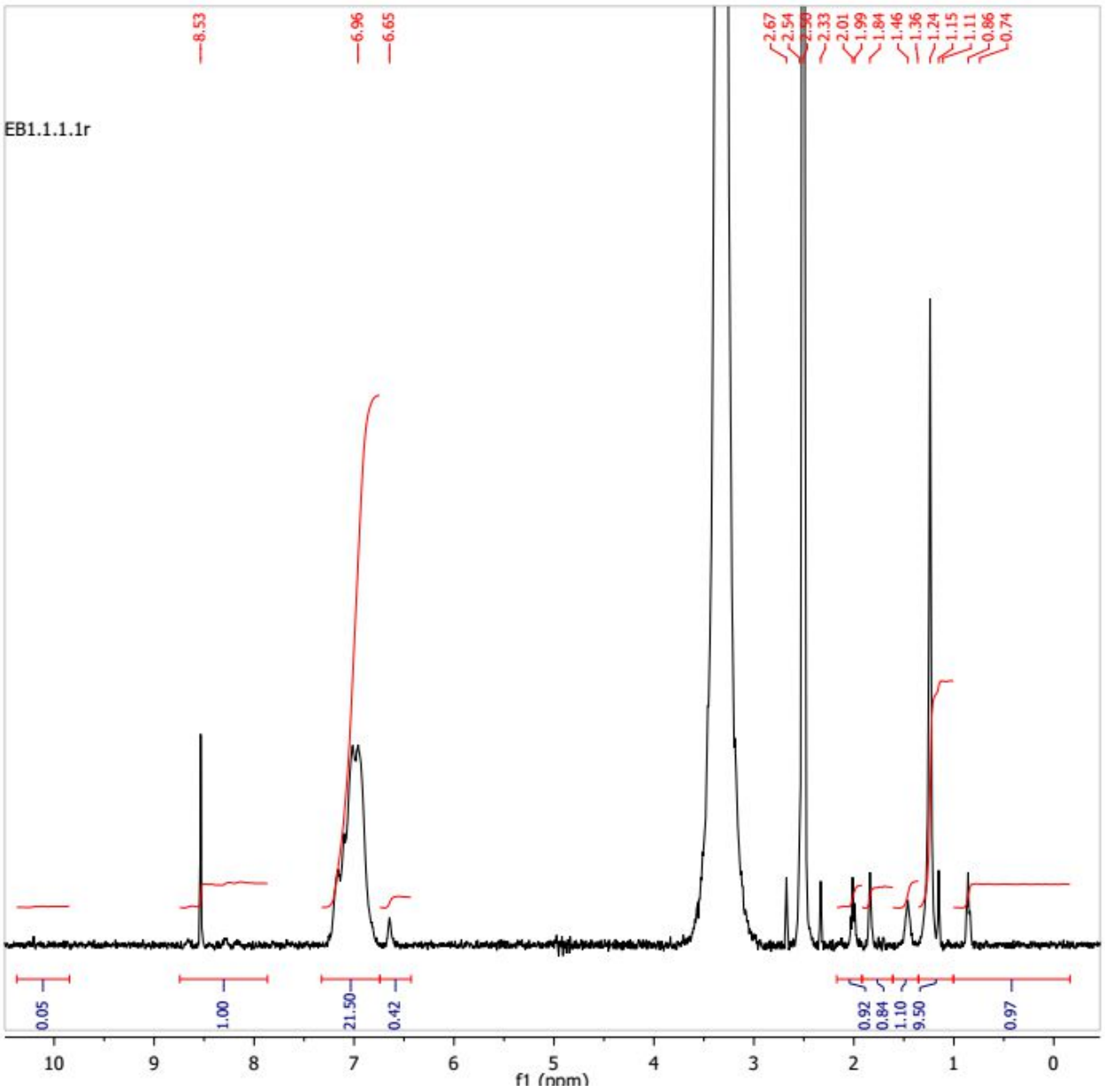

b)

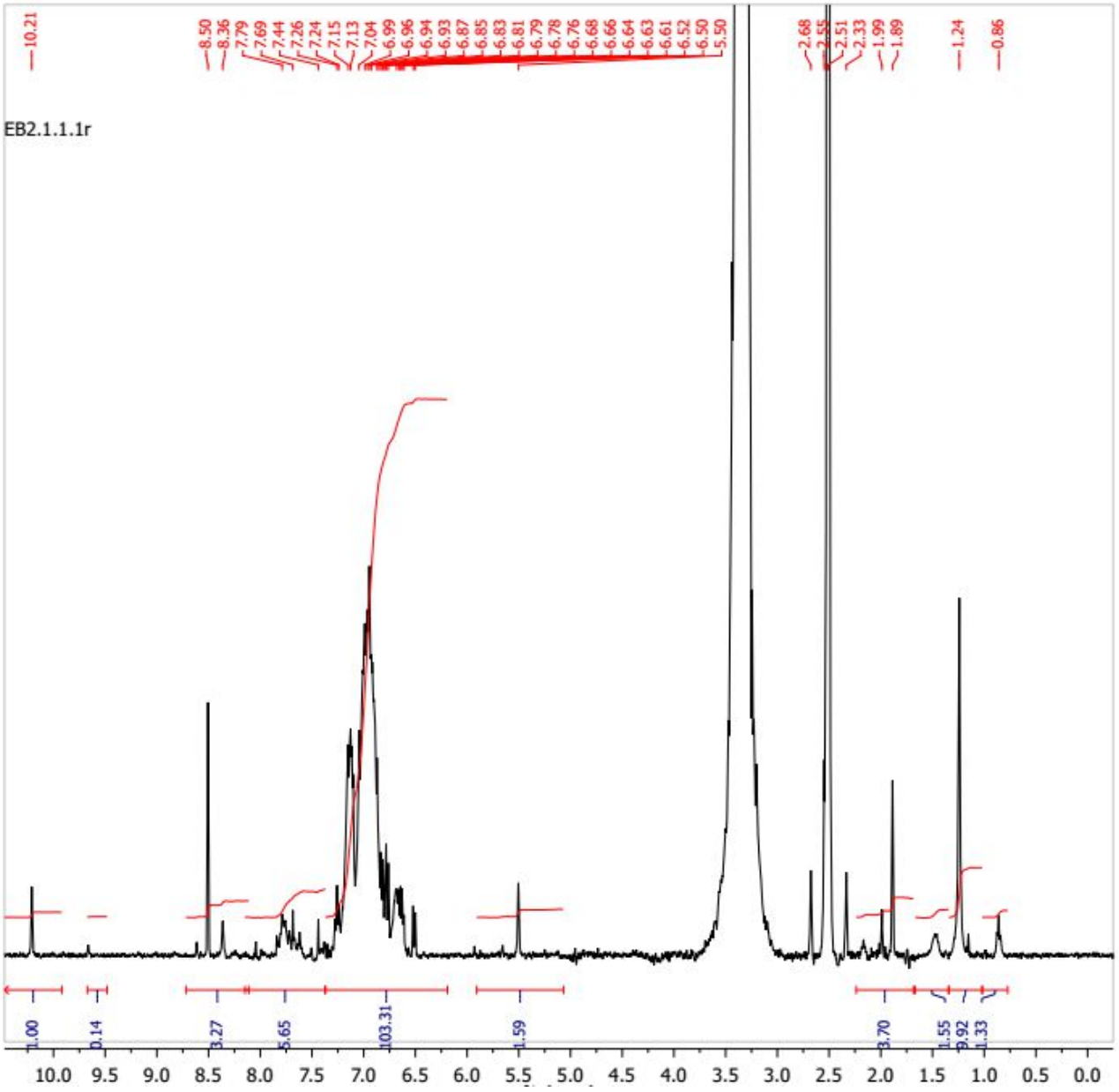

Figure 1: H^1-NMR spectra of a) EB1 b) EB2.

The NMR analyses show interesting features due to the different mechanism of polymerization. While for the traditional polymerization method a typical emeraldine base, EB1, spectrum was obtained, in the case of EB2 a wide variety of peaks, probably due to a side-reaction mechanism due to the presence of H_2O_2, was observed. The signals around 6.5-6.8 (delta) are probably related to the presence of quinonic structures.[12] Moreover, the signal at delta 5.5 can be ascribed to formation of phenol units in the polymeric backbone.

It is known that from H_2O_2 decomposition hydroxyl radical (˙OH) species are produced. These latter could be involved in a competitive reaction involving a first step of addition to the aniline dimer or polymer/oligomer backbone leading to a new radical species (A). The radical species (A) then can

react with another ˙OH leading to hydrogen abstraction to produce phenol units (B),[2] as described in the scheme 1.

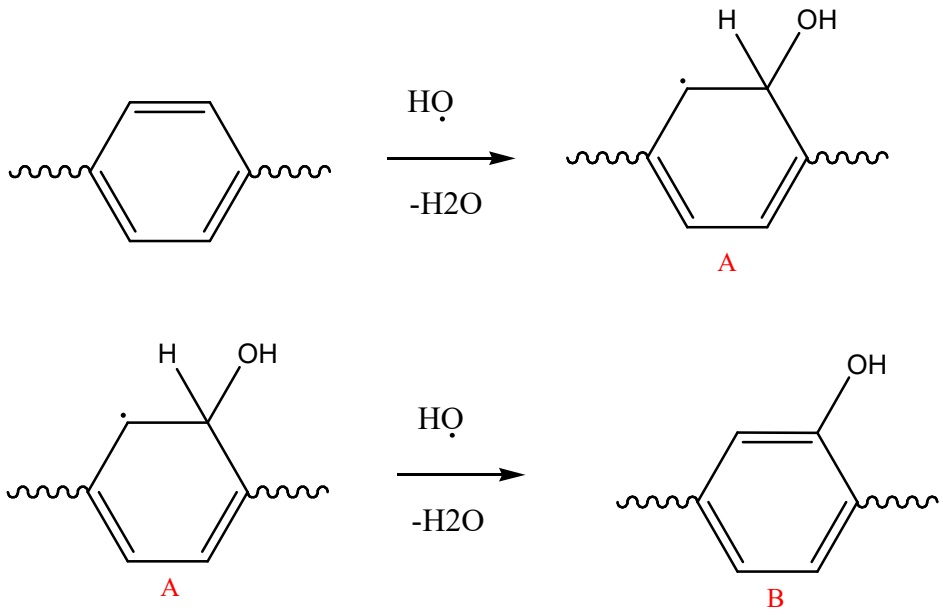

Scheme 1: Proposed reaction mechanism for phenol units formation *via* hydroxyl radical.

A further oxidation of this species could lead to the formation of the benzoquinoid structures that could reduce the regularity of PANI crystalline structure and thus enhancing solubility.

Incorporation of phenolic groups during PANI synthesis using H_2O_2 was already proposed from Blaha *et al.*[13] They reported that the presence of phenolic groups allows PANI self-doping with conductivity decrease.

In Fig. 2 the UV-vis spectra of PANI1/CSA, PANI2/CSA, PANI1/AMSA and PANI2/AMSA in DMSO solution are reported.

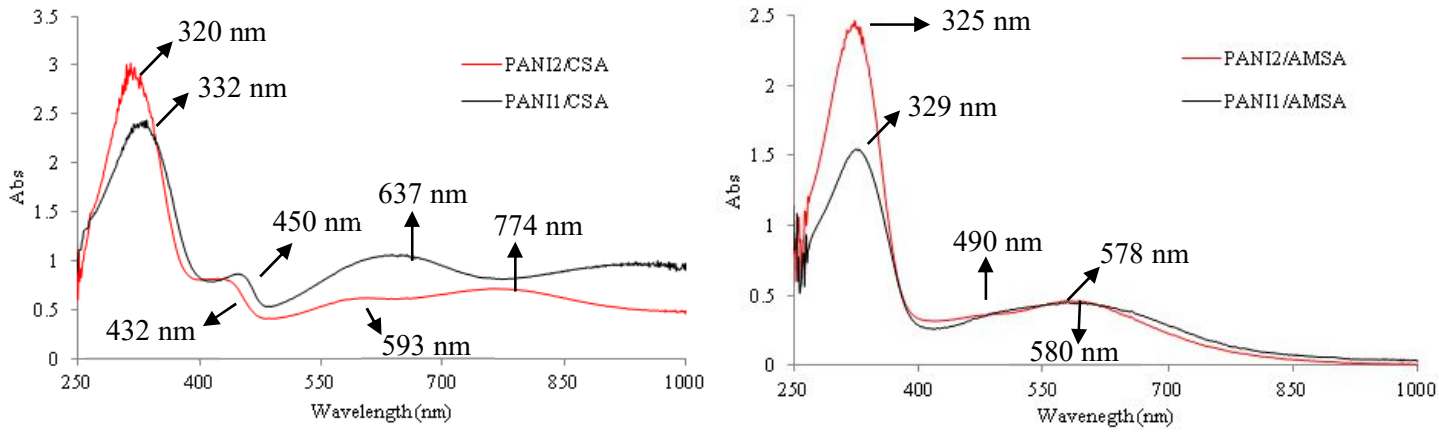

Figure 2: UV-vis spectra of PANI1/CSA and PANI2/CSA (left) and PANI1/AMSA and PANI2/AMSA (right).

All the samples show the characteristic bands of PANI in its emeraldine form. However, a comparison among the four spectra easily points out that the two different types of dopants strongly affect the protonation level of the polymers. In agreement with literature,[20-22] all the spectra reported in Fig. 2 show the band at 320-330 nm assigned to the $\pi \rightarrow \pi^*$ transition of the benzenoid rings. When the dopant of choice is CSA, both the PANI1 and PANI2 samples exhibit a maximum at 430-450 nm attributed to polaron–π^* transition that gives a green color to the solution. This band is independent from the acid used, demonstrating a complete protonation for both the PANIs. In AMSA-doped PANIs spectra the polaron–π^* transition band is weak in intensity and shifted towards higher wavelengths (the solutions of PANIs/AMSA samples resulted light blue). This bathochromic effect can be attributed to many factors: nanostructuration of the materials, conjugation extension,[23] switch from coil-like to expanded conformation of the polymeric chains[24] and disaggregation of the PANI chains in solutions,[25] effects which are consistent with a low degree of protonation, in other words a low grade of doping. Typical benzenoid to quinoid excitonic transition is responsible for bands at higher wavelengths in the electronic spectra of PANI. For PANI in its base form this band is generally centered at 600 nm, whereas for protonated PANI it is shifted at around 800 nm.[26, 27] It is interesting to observe that AMSA-doped PANIs show the typical band of the base form confirming a low protonation level, that will be further discussed in light of conductivity measurements (see § 3.4). On the contrary, the UV-vis spectra of CSA-doped materials are characterized by both bands, the one typical of PANI base (637 nm and 593 nm for PANI1 and PANI2 respectively) and the one of PANI salt (> 850 nm and 774 nm respectively). The bathochromic shift of the benzenoid to quinoid excitonic transition band in the visible region for PANI1 could be ascribed to a change of conformation of polymeric chains from coil-like to rod-like promoted by the repulsion of positive charges causing straightening of the chains.[24] These results demonstrate that AMSA is not able to properly protonate PANI in chloroform, whereas CSA leads to polymers characterized by a protonation level intermediate between PANI base and salt. These results are in agreement with the conductive behavior observed for these materials (see § 3.4).

The FT-IR spectra of all the materials are reported in Fig. 3. All synthesized materials show the characteristic bands of PANI in the form of conductive emeraldine, as confirmed by the characteristics bands at 1573 cm^{-1}, assigned to the C=C stretching of the quinoid rings (N=Q=N), and by the two bands at 1507 cm^{-1} and 1492 cm^{-1} due to the C=C stretching vibration modes of the benzenoid rings (N-B-B).[8] The bands at 1310 cm^{-1} and 1244 cm^{-1} are related to the C-N and C=N stretching modes, whereas the in-plane and out-of-plane bending of C-N is responsible for those at 1038 cm^{-1} and 882 cm^{-1}.[28] The bands at 749 cm^{-1} and 693 cm^{-1} are assigned to the deformation vibration modes for the aromatic rings, while the band at 573 cm^{-1} is typical of 1,4 di-substituted

benzene.[18,23] For CSA-doped PANIs the presence of the doping agent is confirmed by the stretching vibration band at 1737 cm^{-1} typical of the ketonic C=O of CSA, such as by the bands at 1160 cm^{-1}, 752 cm^{-1} and 619 cm^{-1} that can be attributed to S=O, C-S and S-O vibration respectively.

In the FT-IR spectra of AMSA-doped PANIs the typical bands of the dopant are absent, confirming the data obtained by the use of UV-Vis spectroscopy. This suggests that in the conditions used in this work AMSA is not able to completely protonate PANIs. AMSA exists in form of zwitterion as confirmed by literature.[26] It could be argued that the salt is not able to dissolve in chloroform and thus unable to react with the amine group of PANI to obtain protonation.

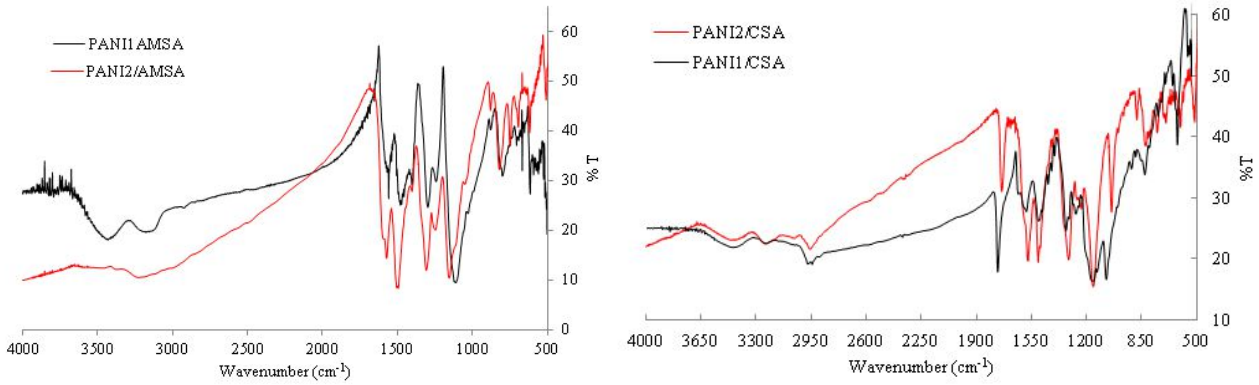

Figure 3: FT-IR spectra of PANI1/CSA, PANI2/CSA, PANI1/AMSA and PANI2/AMSA.

The morphology of each sample was evaluated by scanning electron microscopy and the results are reported in Fig. 4.

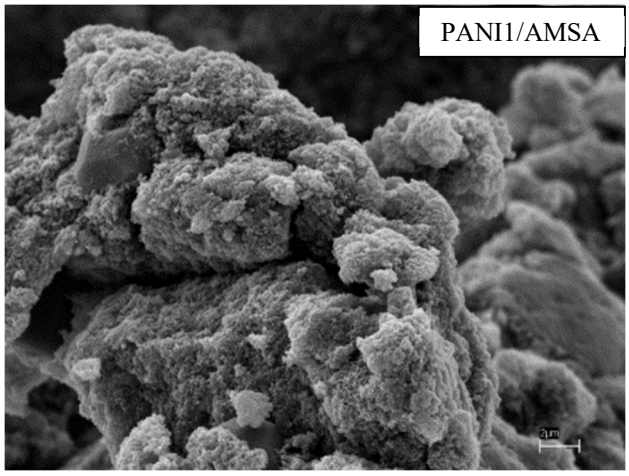

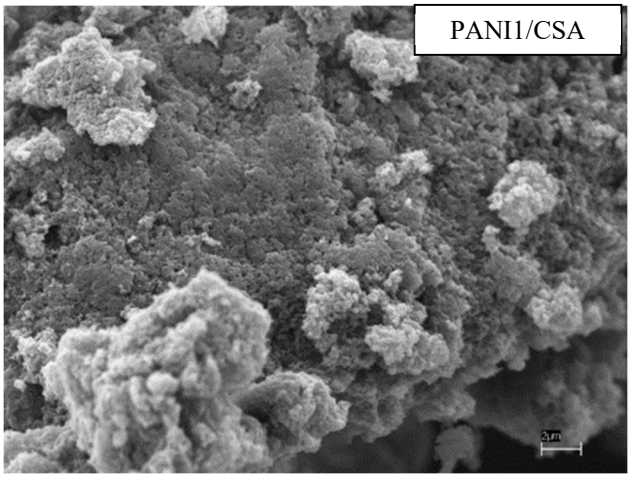

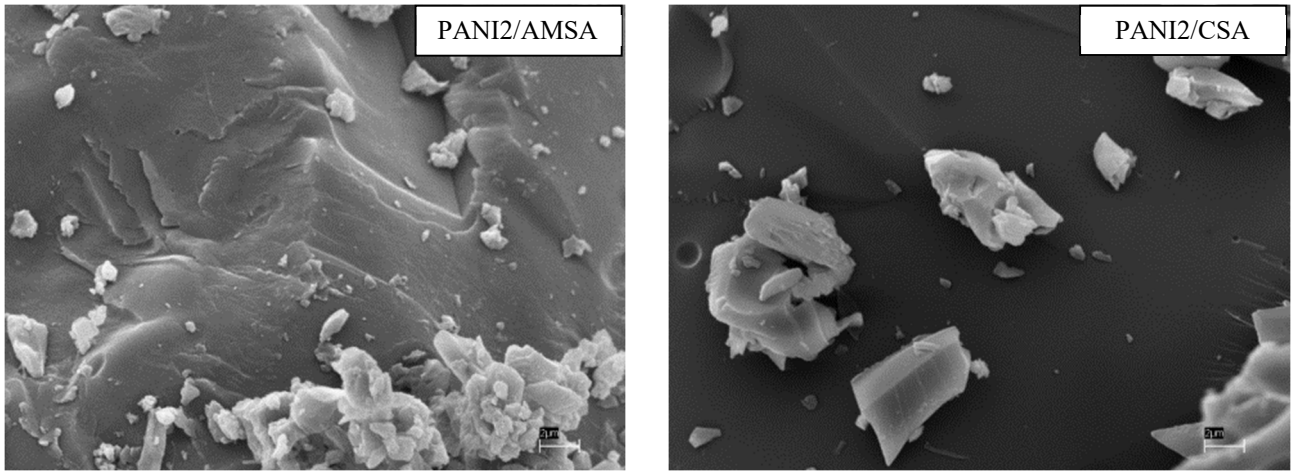

Figure 4: SEM images of PANI1/CSA, PANI2/CSA, PANI1/AMSA and PANI2/AMSA.

The images display that both the PANI1-based materials exhibit more regular rod-like structures and higher porosity if compared with those of PANI2-based polyanilines, characterized by smooth and compact surfaces.

The different morphology of the PANI1 and PANI2 types of polyanilines could be reasonably attributed to the diverse solubility of the two PANI. PANI1 is less soluble than PANI2 and thus is probably present in solution as suspension of submicrometer particles that merges during solvent evaporation. PANI2, because of the phenol/quinoid functionality, is present in solution as single PANI molecule that thus can be able to form compact structure during solvent evaporation.

The atomic surface composition of all the specimens was evaluated by XPS measurements. From the survey scans (Fig. 5) we can detect the presence of C, N and O for all the samples and S for the doped-one only (Table 2). The ratio between sulfur and nitrogen atoms gives a first evaluation of the doping level of the different samples, where a complete doping is achieved when the S/N ratio is 0.5. Since AMSA contains an atom of nitrogen for every atom of sulfur, the doping level should be corrected: *D.L. % = 200*[S] / ([N]-[S]),* which has been applied to compute numbers in Table 2. These results allow to confirm that CSA achieves very high doping levels, complete in the case of PANI1, while AMSA achieves lower doping levels, between 59 and 63 %.

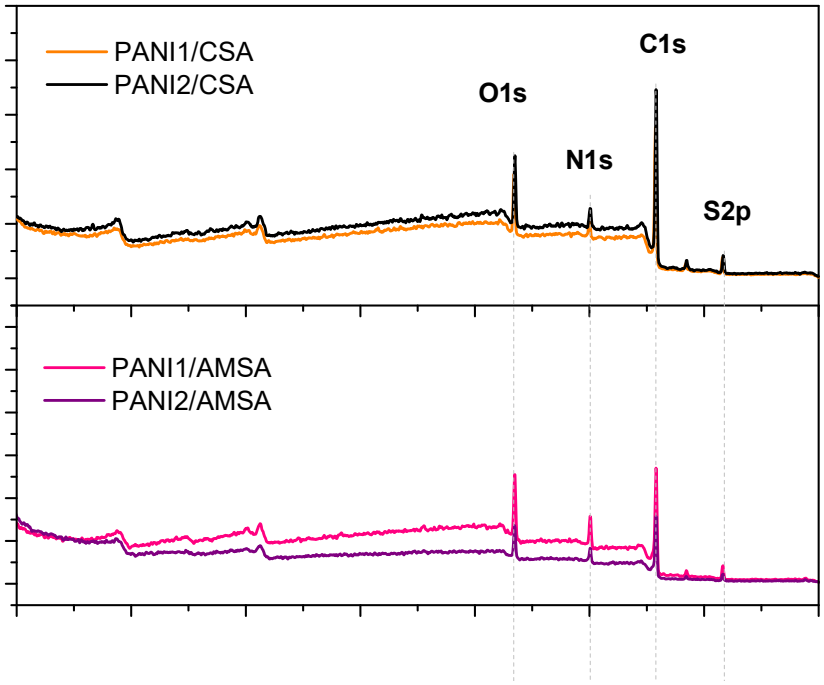

Figure 5: Survey scans for all the samples.

Sample\Atom species	C	O	N	S	Doping level [%]	VBM [eV]
EB1	82.9	2.9	14.2	0.0	-	1.3±0.2
EB2	84.5	2.3	13.2	0.0	-	1.9±0.2
PANI 1/CSA	75.0	15.0	6.6	3.4	100	1.2±0.1
PANI 2/CSA	76.0	13.9	7.0	3.1	89	1.1±0.1
PANI 1/AMSA	67.4	16.9	12.7	2.9	59	1.9±0.1
PANI 2/AMSA	69.8	15.2	12.1	2.9	63	1.8±0.2

Table 2: Data extracted from XPS measurements: concentration of the different atoms expressed as percentage of EB1, EB2, PANI1/CSA, PANI2/CSA, PANI1/AMSA and PANI2/AMSA, and valence band maximum.

To complete the XPS analyses we focused our attention on the valence band region (see Fig. 6), which is the experimental counterpart of the theoretical Density Of States (DOS) structure. The EB-based films show two similar curves in which we can observe the presence of four features: one at about 3

eV, due to C 2p-π band, then C 2p-σ states near 6 and 9 eV and the C 2s band at 13 eV. The doped samples, instead, apart from the already mentioned peaks a bit broadened and shifted towards higher energy, show an intense peak in the 9-11 eV region due to C-N 2p-σ state.[29-31] Another information, which can be related to the electrical characterization of thin films discussed in the following sections, is the valence band maximum (VBM) position. According to literature, the distance between the X-intercept, obtained with a linear fit on the descending part of the signal towards the 0 eV value, which corresponds to the Fermi Energy (E_F) level, and the E_F itself is the VBM value (reported in Table 2). As can be seen in Fig. 5, there are no sustainable DOS structures nearby the Fermi level, which let us infer that the samples are not perfectly conductive. In fact, the VBM is between 1 and 2 eV far from the E_F, typical for semiconducting materials;[32] in particular EB1 has a VBM lower than EB2, and so all CSA-doped PANIs have a VBM lower than all AMSA-doped ones, giving a figure quite well in agreement with the analyses of former XRPD experiments. In any case the PANI2/AMSA and PANI2/CSA are slightly more populated than the PANI1 counterparts around E_F.

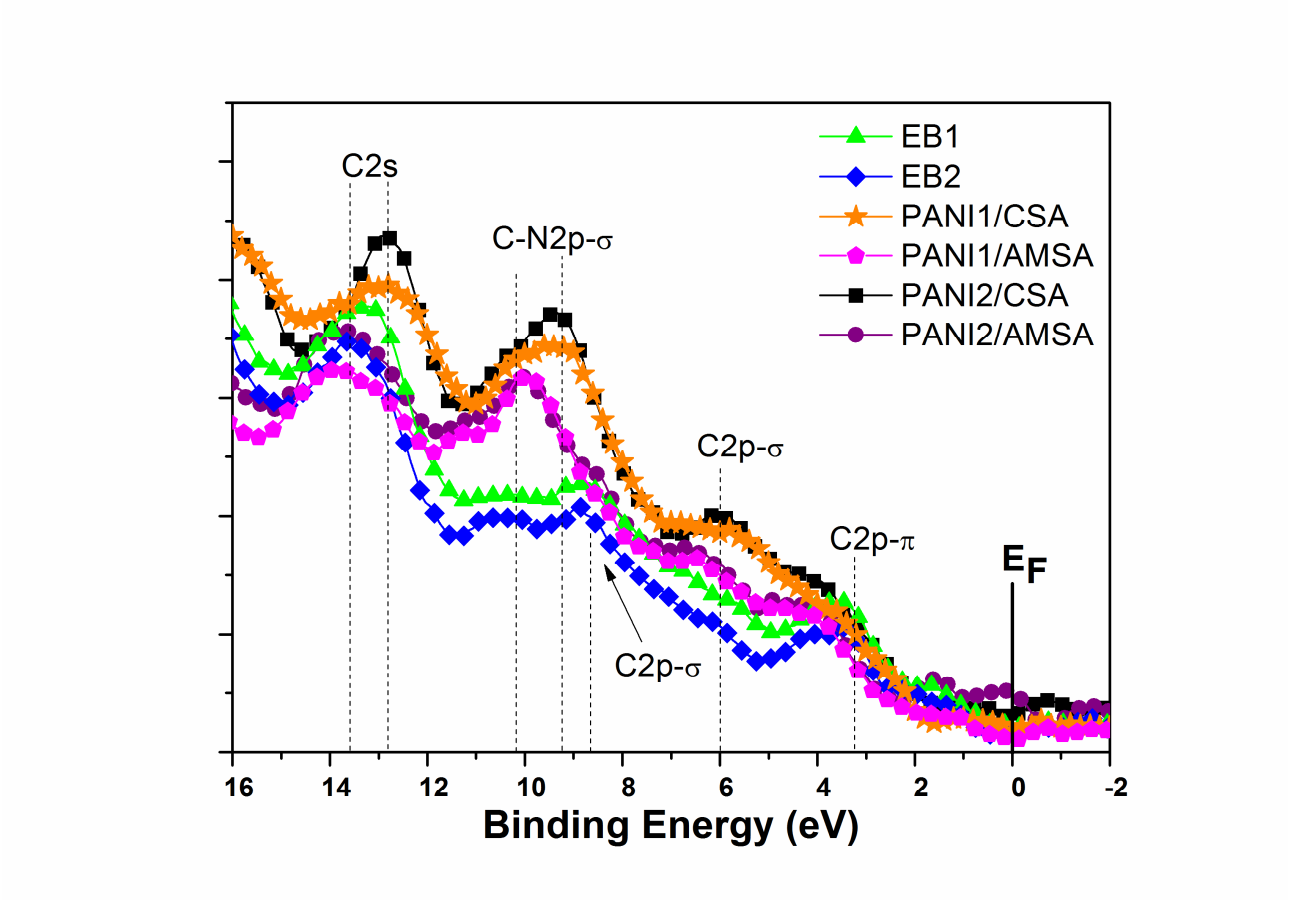

Figure 6: Valence band spectra for all samples. 1 experimental point shown every 3 measured for clarity.

The Fig. 7 shows the schematic representation of the inkjet printed PANI planar device used for electrical characterizations and the inset shows its appearance, it provides mechanical support and a standard electrode spacing for the thin printed films. The gap between Au electrodes, realized on a (100)Si chip by means of optical lithography, is 10 μm, and the chip itself is 7×10 mm^2.

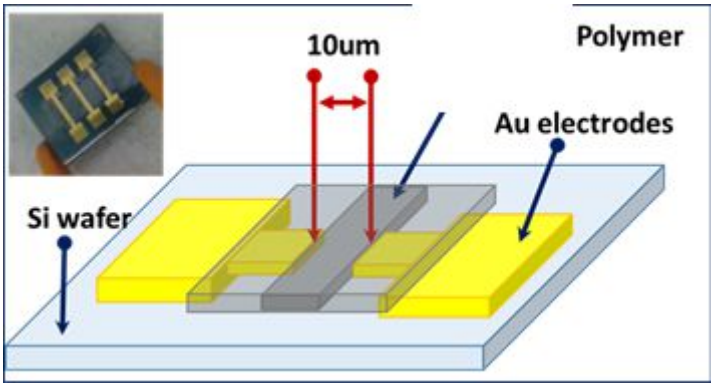

Figure 7: Schematic representation of the planar device, inset: physical device after PANI inkjet printing.

The typical response found in the DC mode shows a slightly nonlinear (deviation from Ohmic behavior typical of semiconductors) dissipative behavior, Fig. 8 (left), in accordance with previous XPS analyses and VBM analysis (Table 2). Samples with a different number of passes for each composition have been printed and characterized, where the number of passes chosen (and hence printability) is inversely proportional to the solubility of the inks: the more soluble an ink is, the less easy it is to create a complete and uniform track. A resume of DC measurements performed on all samples is given in Fig. 8 (right), showing that the best absolute performance is found for PANI2/CSA, which is 6 orders of magnitude more conductive than PANI1/AMSA and 4 more than PANI2/AMSA; PANI1/CSA is found below detection limit (good insulator). This result is only partially in agreement with the XPS Fermi level analyses, suggesting that other properties are influencing more predominantly the DC properties of printed materials, as further discussed in the text (cfr. Table 3).

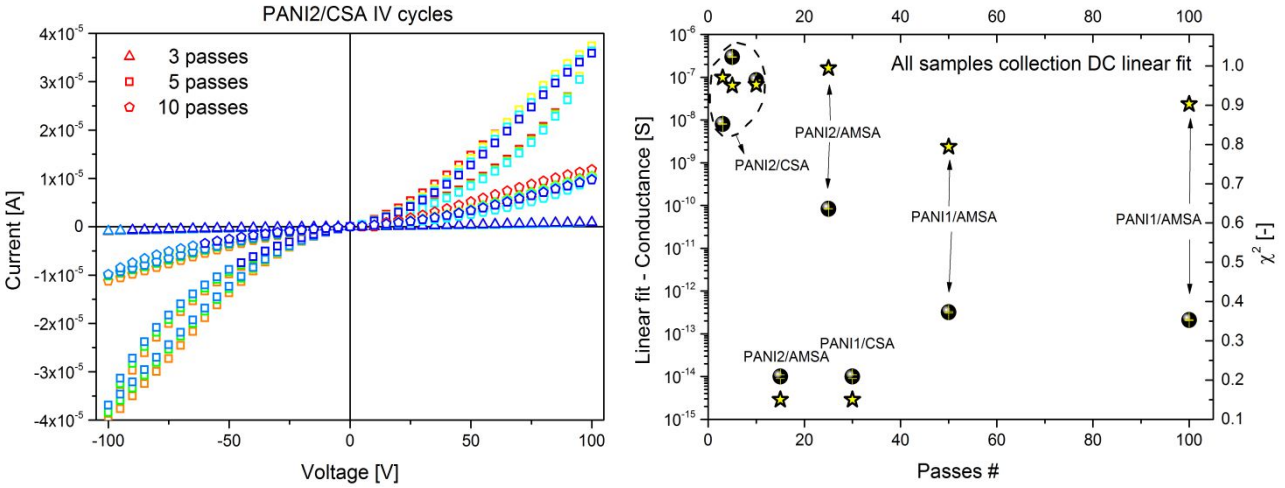

Figure 8: IV cycles in linear scale of sample PANI2/CSA at different number of passes (left). Results from linear fitting of all samples characterized, given in terms of conductance and its associated error and fit quality (right).

The comparison between impedance spectra of samples printed at different number of passes is presented in next four panels (Fig. 9), in the range from 200 kHz to 2 MHz. Apparently, the number of passes is not affecting monotonously impedance curves (cfr. PANI1/CSA and PANI2/AMSA, where increasing the passes produces specular effects, in one case reducing in the other increasing the real component of impedance). Putting the focus on sample PANI2/CSA (Fig. 10, left), we see that in the low frequency range (up to 10 kHz) the system shows capacitive behavior and a marked dependence on the number of passes, probably due to the strong influence of track geometry.[33] Increasing the frequency (Fig. 10 right), the system goes through a transition and recovers a behavior which is less dependent upon the number of passes, as well as convergence already seen in similar systems.[33] The linear part in bilog graphs has been fitted by a universal conduction model,[34] whose global results are given in Fig. 11. The most relevant parameters are σ_0 (AC conductance in the limit for $f \rightarrow 0$ Hz) and the critical exponent c. PANI2/CSA, the most conductive sample according to IV cycles, has the lowest σ_0 conductance and also the less pronounced dependence upon frequency, but the highest critical exponent, around 1.45, while other samples range between 1.35 and 1.10. It is clear that the parameters the least influenced by layer thickness and geometry are both the critical exponent c and the coefficient a.

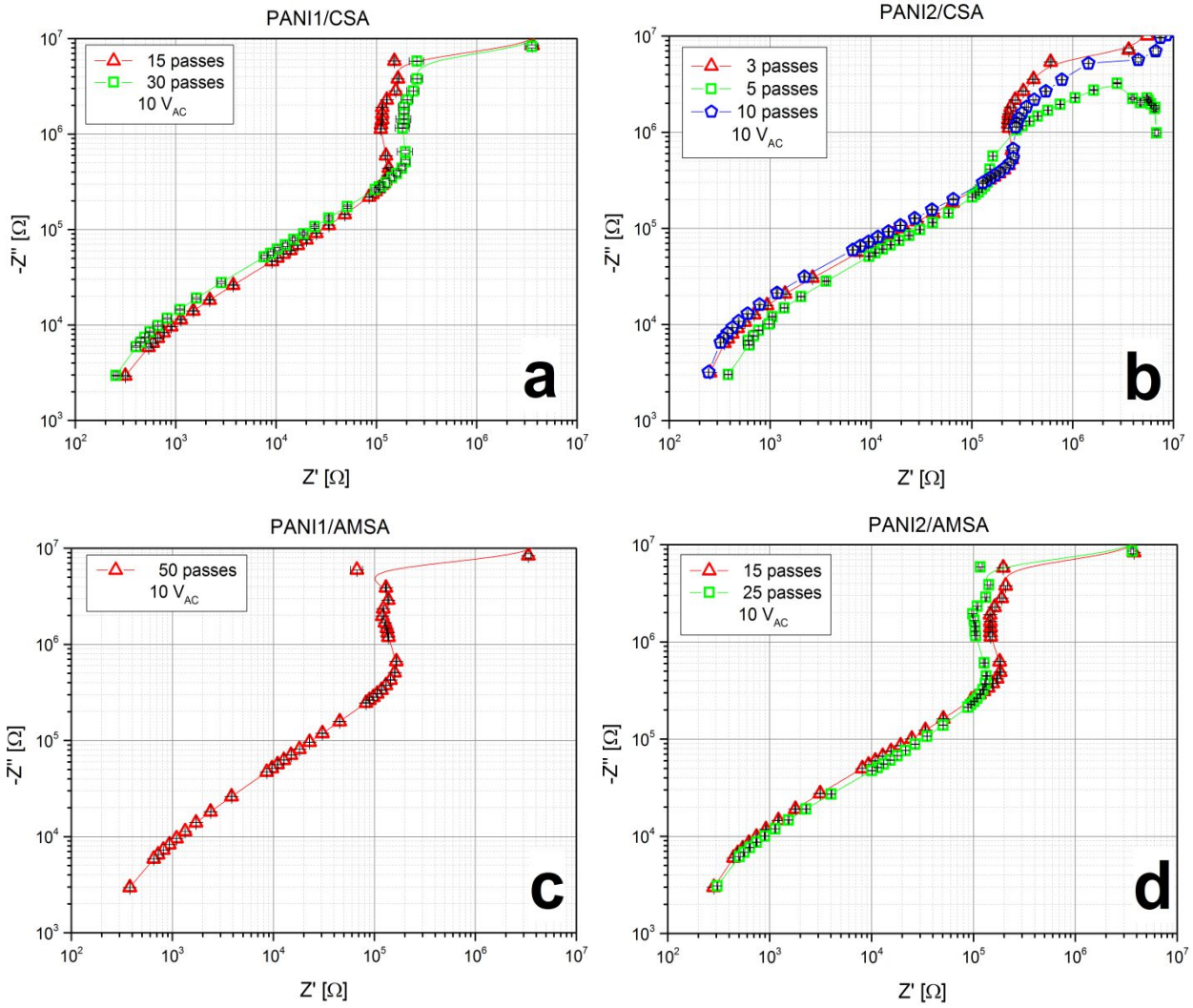

Figure 9: Nyquist plots of inkjet printed PANI: PANI1/CSA (a), PANI2/CSA (b), PANI1/AMSA (c) and PANI2/AMSA (d).

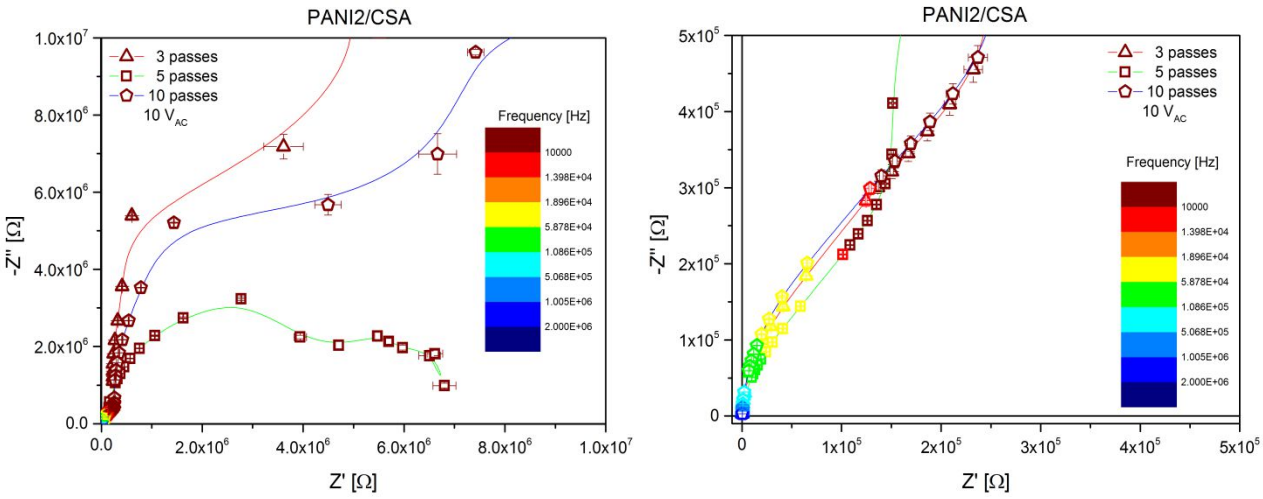

Figure 10: Nyquist plots given in the linear scale for samples PANI2/CSA at different number of passes, focusing on low frequency range (left) and high frequency range (right).

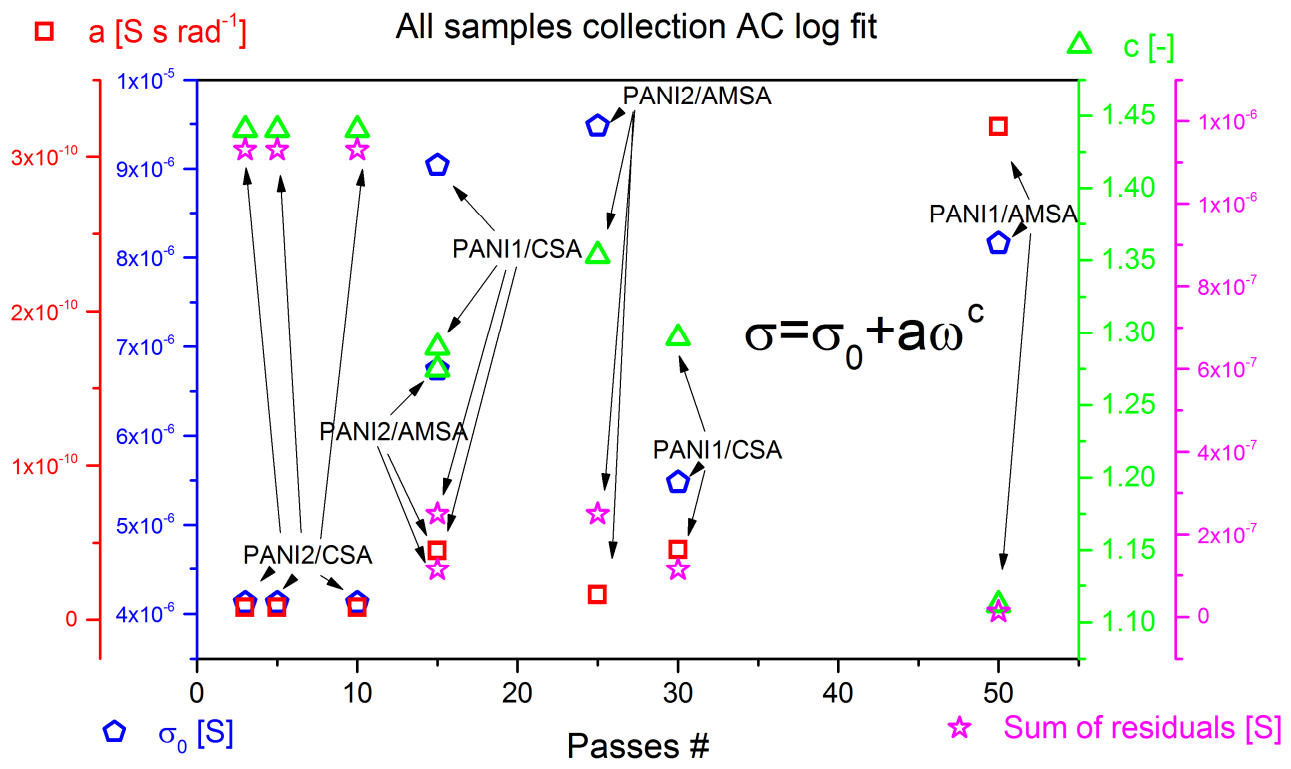

Figure 11: Summary of parameters extrapolated from fitting measurements of Fig. 9 with the universal model in the inset. The three pure fit parameters are shown together with the sum of residuals, showing a slight deviation from ideality only in the case of samples PANI2/CSA.

So far, in order to better understand the influence of material properties towards electric properties of printed patterns, we have summarized qualitative data in Table 3 and evidenced polarity trends; DC conductivity and the critical exponent are a direct consequence of the measured solubility of the four samples, while AC zero frequency conductivity is a direct consequence of the practical printability of thin films. Doping level, VBM and protonation level still appear to be less significant parameters towards the achievement of better figures of merit.

Properties\Sample	PANI1/CSA	PANI2/CSA	PANI1/AMSA	PANI2/AMSA
Solubility (real) [g l^{-1}]	-	++	--	+
Printability (max # passes achieved)	+	--	++	-
Doping level (XPS)	++	+	--	-
VBM (XPS)	++	+	--	-

Protonation (UV-Vis)	++	+	--	-
DC conductivity / (mg/ml * # passes) [S l g^{-1}]	-- ($o10^{-13}$)	++ ($o10^{-6}$)	- ($o10^{-11}$)	+ ($o10^{-10}$)
AC conductivity @ $f \rightarrow 0$ / (mg/ml * # passes) [S l g^{-1}]	+ ($o10^{-4}$)	-- ($o10^{-5}$)	++ ($o10^{-3}$)	- ($o10^{-4}$)
Critical exponent [-]	-	++	--	+

Table 3: Summary of key properties reported as qualitative summer, where the background cell colors evidence three polarities and better help the reader to correlate the materials properties with the functional figures of merit.

A further analysis is performed submitting a DC bias [-40, +40] V jammed with an AC signal (1 V_{pp}). The reason for applying a DC bias bigger than the signal is to understand if such samples can be operated as voltage controlled impedance and explore states where the differential impedance changes sign. Sample PANI2/CSA properties are shown in Fig. 11 and compared to sample PANI2/AMSA, as a representative of less conductive materials, in Fig. 12. Almost no hysteresis is seen and a slight separation between states at high negative (positive) biases is found. The most interesting properties are represented by: i) the polydromicity of the impedance states, found for every sample at every frequency; ii) a variable sign differential impedance at 1 MHz in sample PANI2/AMSA (Fig. 12d), where it is possible to change the sign of resistance from positive (@ ±40 V) to negative (@ ±35 V or ±5 V).

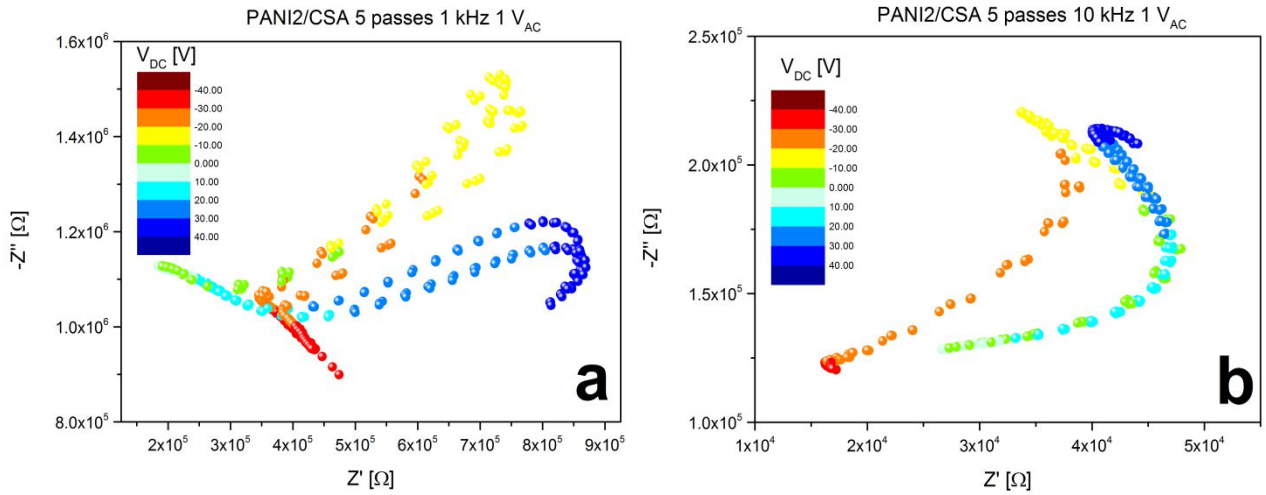

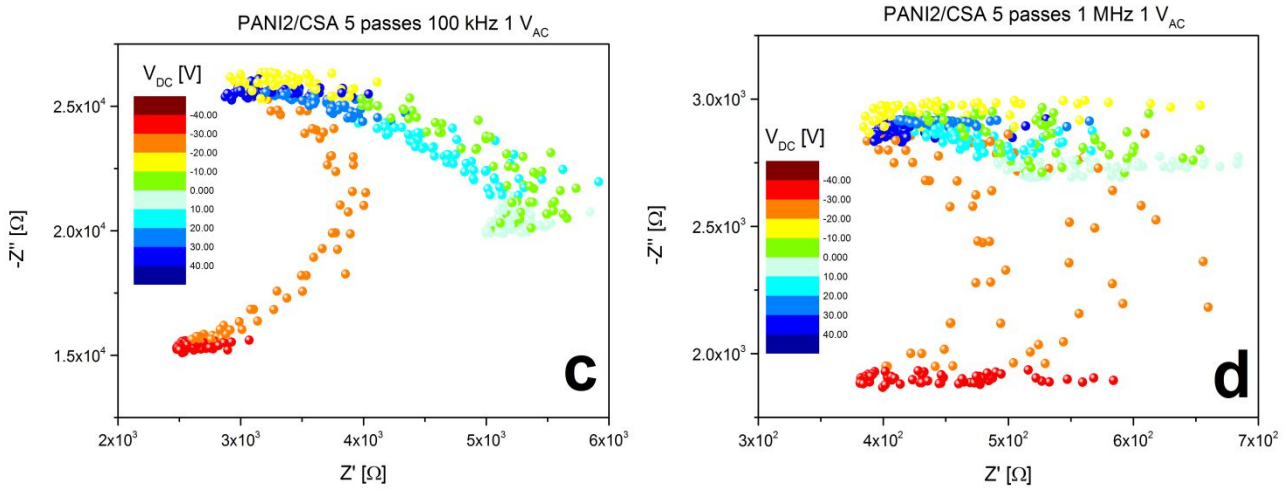

Figure 12: Sample PANI2/CSA (5 printed passes), curves taken at 1 (a), 10 (b), 100 (c) and 1000 kHz (d), under 1 V_{pp} and a DC bias cycling between -40 and +40 V.

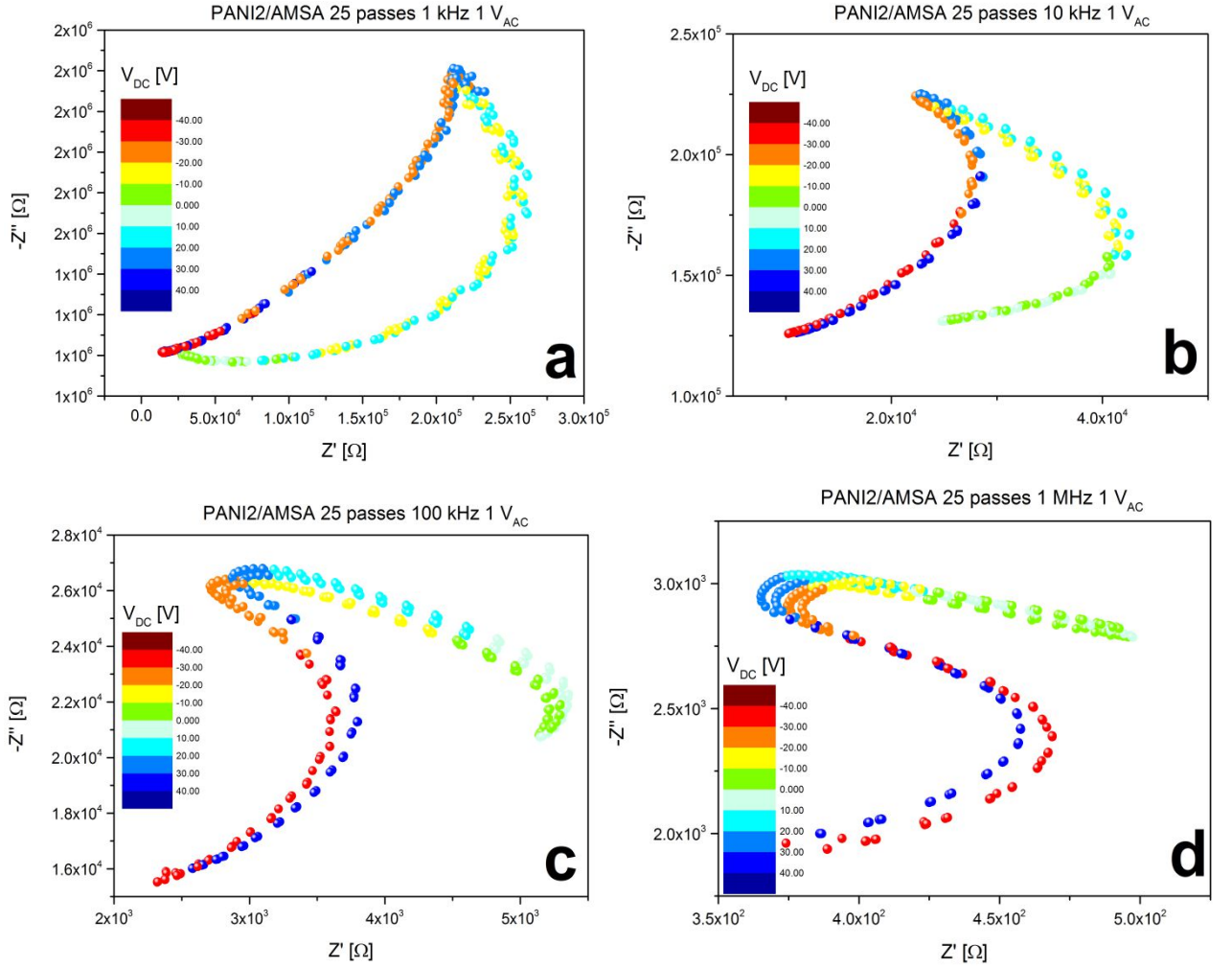

Figure 12: Sample PANI2/AMSA (25 printed passes), curves taken at 1 (a), 10 (b), 100 (c) and 1000 kHz (d), under 1 V_{pp} and a DC bias cycling between -40 and +40 V.

Hysteresis is studied by analyzing Bode plots, where resistance and reactance are simply on the same graph, represented as a function of DC bias. The four panels of Fig. 13 show the response of PANI2/CSA, revealing a clear asymmetry and a quite high noise floor level, above 100 kHz. The four panels of Fig. 14 show the response of PANI1/AMSA, that we found quite representative also of PANI1/CSA and PANI2/AMSA behavior. Here the noise level is much lower, all measures being clear and definite up to 1 MHz; furthermore i) hysteresis opens at 10 kHz, growing in area as a function of frequency, and ii) branches with a change in sign of differential resistance (reactance) are clearly seen. Such features have already been observed on similar PANI-based systems.[37]

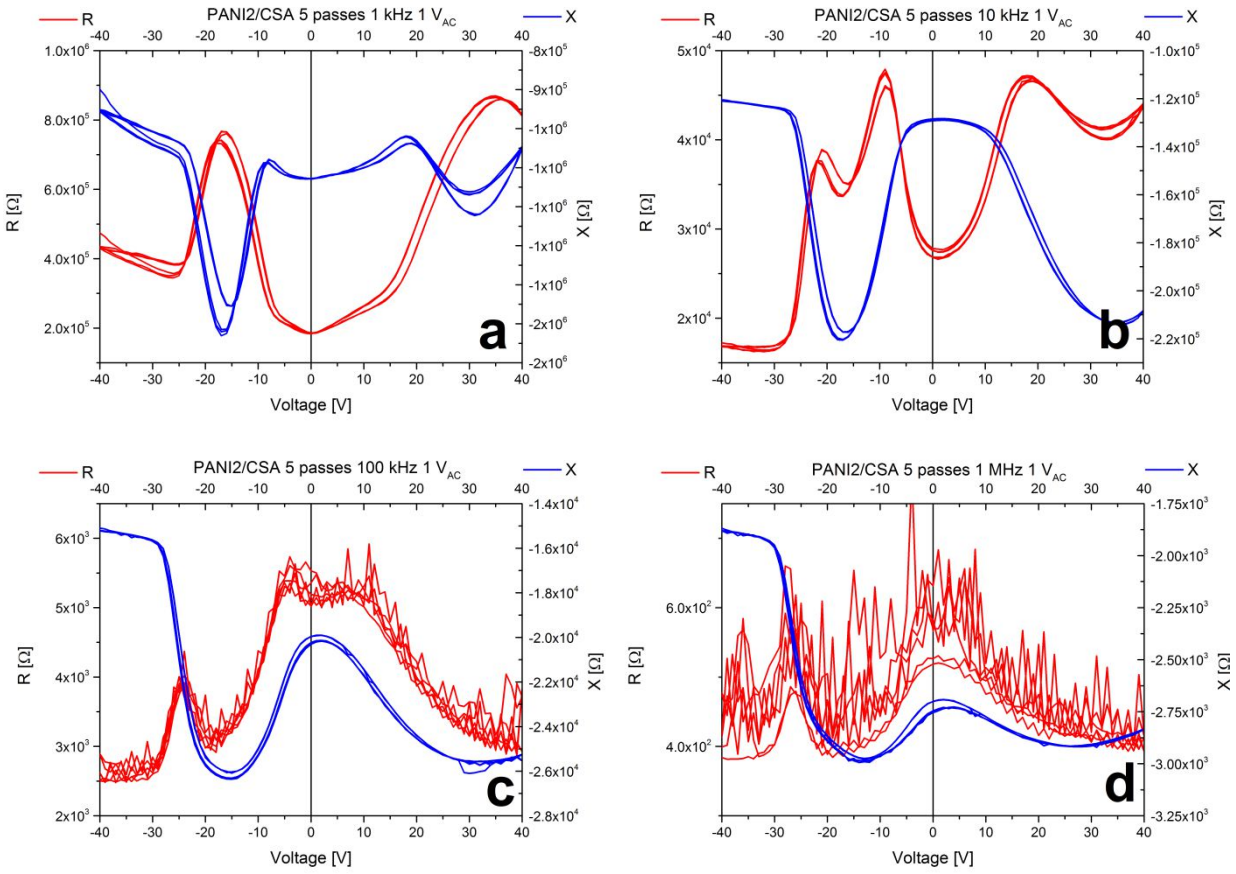

Figure 13: Sample PANI2/CSA (5 printed passes), Bode plots of the hysteresis measurements, showing real and imaginary parts of the impedance as a function of signal frequency: 1 (a), 10 (b), 100 (c) and 1000 kHz (d), under 1 V_{pp} and a DC bias cycling between -40 and +40 V.

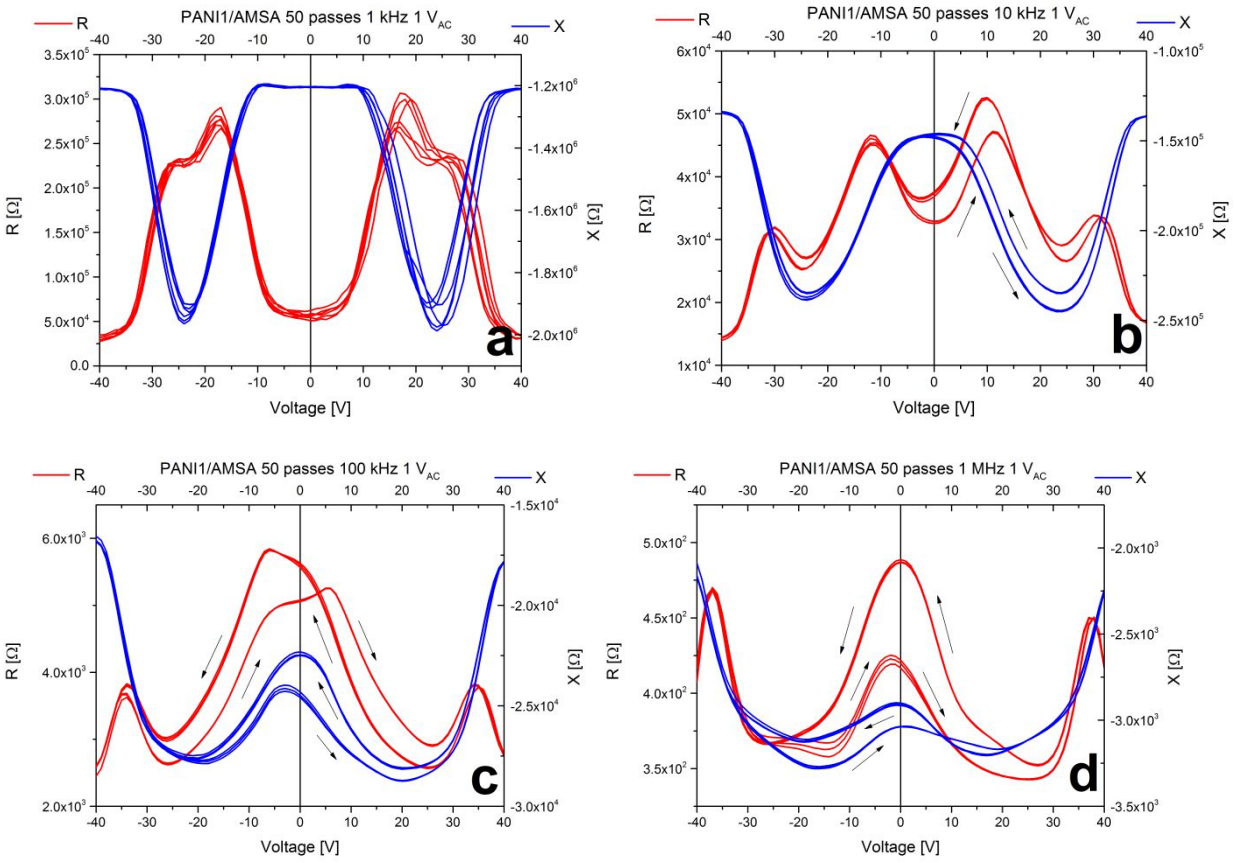

Figure 14: Sample PANI1/AMSA (50 printed passes), Bode plots of the hysteresis measurements, showing real and imaginary parts of the impedance as a function of signal frequency: 1 (a), 10 (b), 100 (c) and 1000 kHz (d), under 1 V_{pp} and a DC bias cycling between -40 and +40 V.

Conclusions

Doped PANIs prepared using an innovative green method were used to formulate inks for inkjet printing functional devices. The obtained inks were compared with the equivalent inks prepared using doped PANIs synthesized by a traditional method. PANIs obtained using the innovative method more soluble in DMSO, such irregularities are related to secondary reactions that allow the formation of quinones and phenolic groups on the main polymer chain. Protonation level, doping level, valence band maximum have been assessed on the basis of NMR, UV-Vis, FTIR and XPS measurements. Functional properties have been measured on inkjet printed thin films, in the DC and AC regime, including bias measurements to assess hysteresis. We have seen that the absolute conductivity (as directly measured in the DC regime or extrapolated through the universal fit in the AC regime) is poorly correlated to structural properties, and we have shown how important are features such as solubility and printability, in order to achieve higher functional figures of merit. Other features, such

as the critical exponent of the universal model and the hysteresis opening, are less influenced by the geometry of the sample and the number of printed passes.

Conflicts of interest

There are no conflicts to declare.

Acknowledgements

We would like to thank the Università degli Studi Milano for supporting this research by the *Piano di Sostegno alla Ricerca – 2016 - Linea 2 Azione A*, *Project n. 18386*

References

[1] T. H. Qazi, R. Rai, A. R. Boccaccini, *Biomaterials*, **35** (33), 2014, 9068-9086.

[2] Y. Wu, Y. X. Chen, J. Yan, S. Yang, P. Dong, P. Soman, *J.Mater.Chem.B,* **3**, 2015, 5352-5360.

[3] J. Stejskal, M. Trchová, P. Bober, P. Humpolíček, V. Kašpárková, I. Sapurina, M. A. Shishov, M. Varga. *Conducting Polymers: Polyaniline. Encyclopedia Of Polymer Science and Technology*, Wiley, Hoboken, 2015, 1–44.

[4] E. M. Geniès, J. F. Penneau, M. Lapkowski, A. Boyle, *J. Electroanal. Chem. Interfacial Electrochem.*, **269**, 1989, 63–75.

[5] A. Kitani, J. Yano, A. Kunai, K. Sasaki, *J. Electroanal. Chem. Interfacial Electrochem.*, **221**, 1987, 69–82.

[6] S. Bocchini, A. Chiolerio, S. Porro, D. Accardo, N. Garino, K. Bejtka, D. Perrone, C. F. Pirri, *J. Mater. Chem. C*, **1**, 2013, 5101-5109.

[7] A. Chiolerio, S. Bocchini, S. Porro, *Adv. Funct. Mater*., **22**, 2014, 3375-3383.

[8] Z. Chen, C. Della Pina, E. Falletta, M. Rossi, *J. Catal*., **267**, 2009, 93–96.

[9] C. Della Pina, M. Rossi, A. M. Ferretti, A. Ponti, M. Lo Faro, E. Falletta, *Synth. Met*., **162**, 2012, 2250–2258.

[10] C. Della Pina, A. M. Ferretti, A. Ponti, E. Falletta, Compos. *Sci. Technol*., **110**, 2015, 138–44.

[11] E. Falletta, C. Della Pina, M. Rossi, *J. Adv. Catal. Sci. Technol*., **1**, 2014, 6–14.

[12] E. C. Venancio, P.-C. Wang, A.G. MacDiarmid, *Synth. Met*., **156**(5-6), 2006, 357-369.

[13] M. Bláha, J. Zedník, J. Vohlídal, *Polym. Int*., **64**, 2015, 1801-1807.

[14] M. M. Ayad, A. F. Rehab, I. S. El-Hallag, W. A. Amer, *Eur. Polym. J*., **43**, 2007, 2540-2549.

[15] M. Trchová, Z. Morávková, I. Šeděnková, J. Stejskal, Chem. Pap., 66(5), 2012, 415-445.

[16] J. N. Pereira, P. Vieira, A. Ferreira, A. J. Paleo, J. G. Rocha, S. Lanceros-Méndez, J. Polym. Res., 2012, 19:9815.

[17] C. Della Pina, E. Zappa, G. Busca, P. Costa, S. Lanceros-Mendéz, A. Sironi, E. Falletta, *Key Eng. Mat.*, **644**, 2015, 157-162.

[18] E. Falletta, P. Costa, C. Della Pina, S. Lanceros-Mendez, *Sens&Act A*, **220**, 2014, 13-21.

[19] C. Della Pina, E. Zappa, G. Busca, E. Falletta, *Sens&Actuat B*, **201**, 2014, 395-401.

[20] W. S. Huang, A. G. MacDiarmid, *Polymer*, **34**, 1993, 1833-1845.

[21] J. Y. Shimano, A. G. MacDiarmid, *Synth. Met*., **123**, 2001, 251-262.

[22] M.-Y. Hua, G.-W. Hwang, Y.-H. Chuang, S.-A. Chen, R.-Y. Tsai, *Macromolecules*, **33**, 2000, 6235-6238.

[23] S. E. Moulton, P. C. Innis, L. A. P. Kane-Maguire, O. Ngamna, G. Wallace, *Curr. Appl. Phys*., **4**(2–4), 2004, 402–406.

[24] J. Laska, *J. Mol. Struct*., **701**(1–3), 2004, 13–18.

[25] W. Zheng, Y. Min, A.G. MacDiarmid, M. Angelopoulos, Y.H. Liao, A.J. Epstein, *Synth. Met*., **84**(1–3), 1997, 109–110.

[26] A. J. Epstein, J. M. Ginder, F. Zuo, R. W. Bigelow, H. S Woo, D. B. Tanner, A. F. Richter, W.-S- Huang, A. G. MacDiarmid, *Synth. Met*., **18**(1–3), 1987, 303–309.

[27] E. M. Conwell, C. B. Duke, A. Paton, S. Jeyadev, *J. Chem. Phys*., **88**(5), 1988, 3331–3337.

[28] X. Feng, C. Mao, G. Yang, W. Hou, J. Zhu, *Langmuir*, **22**(9), 2006, 4384–4389.

[29] D. Dupont, E. Renders, S. Raiguel, K. Binnemans, *Chem.Commun*., **52**, 2016, 7032-7035.

[30] W. Łużny, M. Śniechowski, J. Laska, *Synth. Met*., **126**(1), 2002, 27–35.

[31] M. Scardamaglia, C. Struzzi, F. J. Aparicio Rebollo, P. De Marco, P. R. Mudimela, J.-F. Colomer, M. Amati, L. Gregoratti, L. Petaccia, R. Snyders, C. Bittencourt, *Carbon*, **83**, 2015, 118-127.

[32] S. Golczak, A. Kanciurzewska, M. Fahlman, K. Langer, J. J. Langer, *Solid State Ionics*, **179**, 2008, 2234–2239.

[33] G. Beamson, D. Briggs, High Resolution XPS of Organic Polymers - The Scienta ESCA300 Database Wiley Interscience, 1992.

[34] A P Monkman, D. Bloor, G. C: Stevens, J. C: H. Stevens, *J. Phys. D: Appl. Phys*., **20**, 1987, 1337-1 345;

[35] A. Chiolerio, S. Bocchini, F. Scaravaggi, S. Porro, D. Perrone, D. Beretta, M. Caironi, C. F. Pirri, *Semicond. Sci. Techn*., **30**, 2015, 104001 (10pp).

[36] V. J. Babu, S. Vempati, S. Ramakrishna, *Mater. Sci. Appl*., **4**(1), 2013, 1-10.

[37] A. Chiolerio, S. Bocchini, M. Crepaldi, K. Bejtka, C. F. Pirri, *Synth. Met*., **229**, 2017, 72-81.